Neuron, Volume *81*
Supplemental Information

Oscillatory Dynamics and Place Field Maps Reflect Hippocampal Ensemble Processing of Sequence and Place Memory under NMDA Receptor Control

Henrique O. Cabral, Martin Vinck, Celine Fouquet, Cyriel M.A. Pennartz, Laure Rondi-Reig, and Francesco P. Battaglia

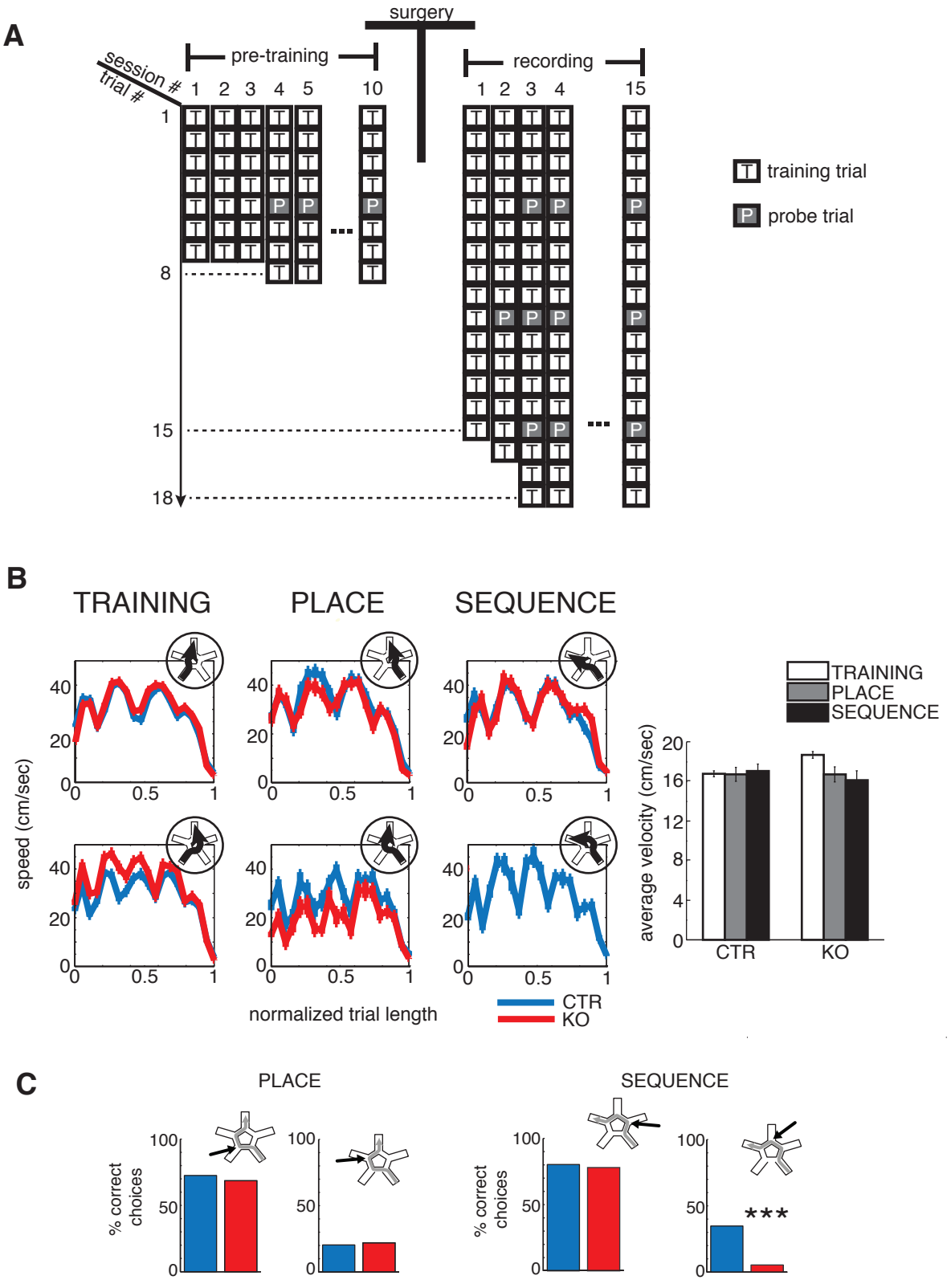

Figure S1. Behavioral schedule and performance, Related to Figure 1.

(A) The order of training and probe trial in each pre-training and recording session, is displayed here.

Before surgery, all mice were subjected to a pre-training protocol, which aimed at getting them familiarized with the task rules. Per batch, two mice (one CTR and one KO) were

selected for study in parallel and implanted with a tetrode carrying drive. Upon recovery, recordings started, with a novel cue set surrounding the maze.

Probe trials were introduced on the 4th session of the pre-training period and on the 2nd session of the recording period, with the total number of training trials being constant.

(B) Left: Speed profiles along the normalized trial length (from departure point to goal point), per trial type. 'Short' paths are shown in the top row, 'long' paths in the bottom one. Local minima correspond to the intersections in the maze.

Right: Average velocity per trial type. There was no difference in the average velocity in the different trial types (ANOVA, n.s.)

(C) Left: Percentage of 'correct' choices at the second (left) and third intersection in long (right) place-strategy trials. There was no difference between genotypes ($\chi 2$--test (between genotypes) n.s.). Note that here a 'correct' choice towards a long place-strategy trial means taking the central alley (i.e. the side of the pentagon). The opposite choice (i.e., taking the radial arm, for the purpose of this analysis marked as an error) results in a successful short SEQUENCE-strategy trial, which is the most probable occurrence for both genotypes. This explains why both genotypes show a relatively low number of 'correct' choices

Right: Same as at left, but for long sequence-strategy trials. A similar ambiguity as in the previous case exists between long sequence and short place-strategy probe trials, resulting in a fraction of correct choices below 50%. Here, however, there was a significant difference between genotypes at the third intersection ($\chi 2$-test (between genotypes) $P < 0.001$).

These results highlight the deficit of NR1-KO mice in using the long sequence trajectory.

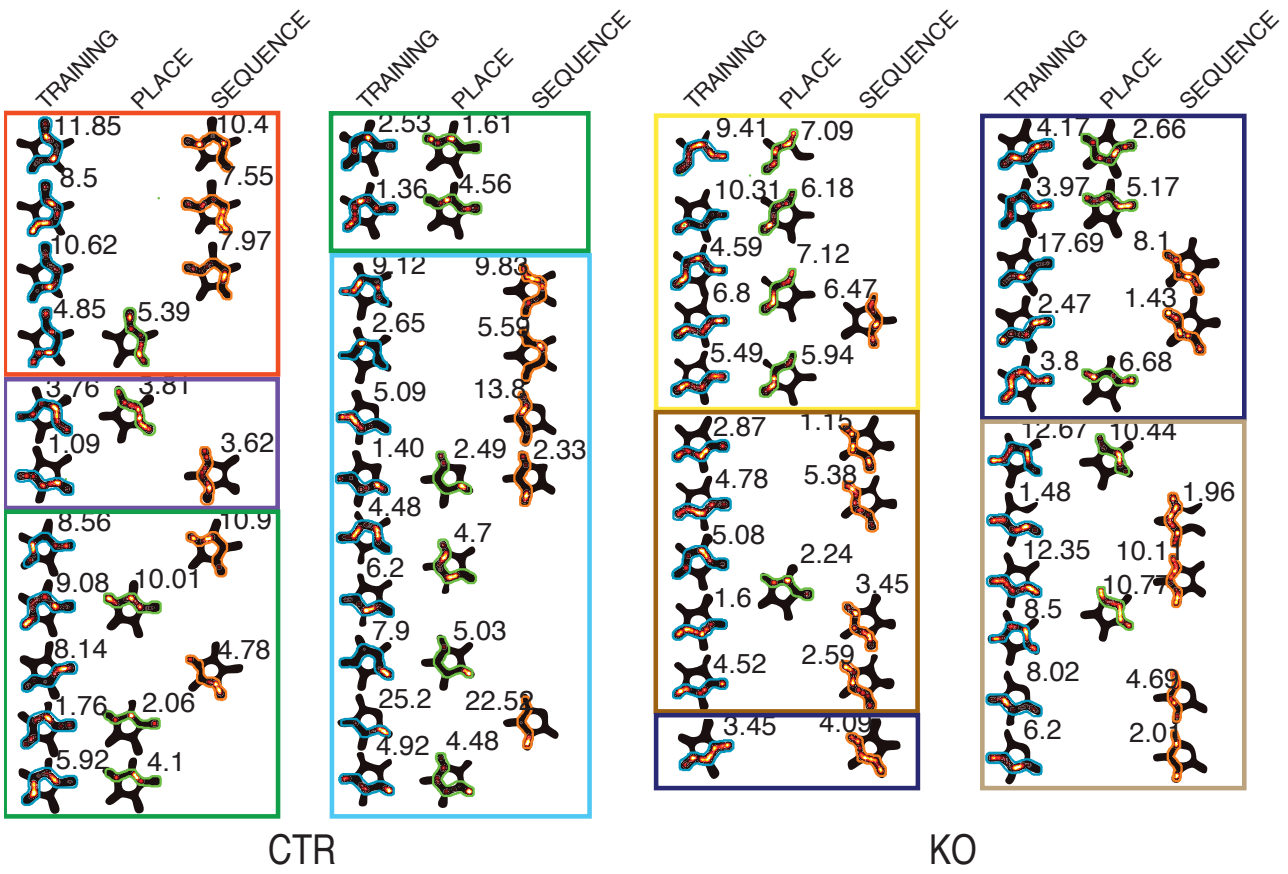

Figure S2. Further examples of place fields in training trials, SEQUENCE- and PLACE-strategy probe trials, Related to Figure 2.

Further examples of firing maps in training trials and probe trials for each recorded animal; Left: CTR, Right: NR1-KO; colors of squares enclosing firing maps denote different animals. Curly brackets indicate sessions, in which both short and long training trials are shown. Firing maps are only shown for arms that were visited by the mouse.

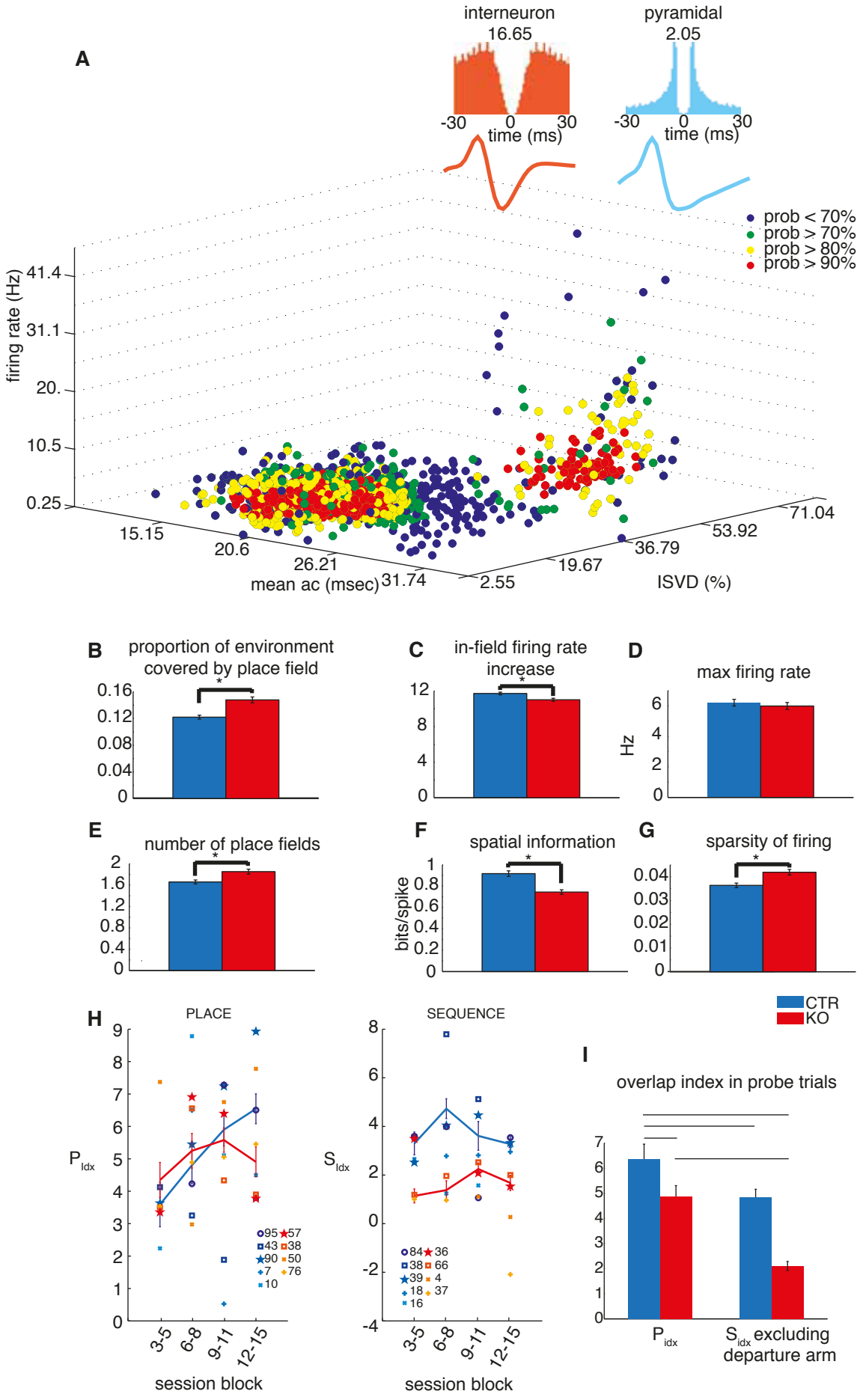

Figure S3. Basic properties of pyramidal cells and interneurons, Related to Figure 3.

(A) Classification of recorded neurons into pyramidal neurons and interneurons. Firing rate, the mean of the autocorrelogram (ac) and the ISVD (initial slope of valley decay; Lansink et al. 2010) yielded good separation of cells in two clusters identifiable with pyramidal cells and interneurons, respectively. By means of a fuzzy clustering algorithm, we defined two clusters and computed the probability of each cell belonging to either clusters (color coded in figure). Each dot represents one isolated neuron; the color indicates the probability of belonging to one of the two clusters. Only neurons with a probability > 70% of belonging to one of the clusters were used in the analysis. Top: the spike waveform of a putative interneuron and a putative pyramidal neuron, with the corresponding autocorrelogram and firing rate (on top of the autocorrelogram) exemplify the separation of these two neuronal types into two different groups using these three measures.

(B) Proportion of environment covered by place field (C) In-field firing rate increase. (D) Maximum firing rate within place field (E) Number of place fields. (F) Spatial information. (G) Sparsity of firing. CTRs shown in blue, NR1-KO in red. NR1-KO place cells show moderately larger (B) and less specific place fields (C and G), have on average more place fields per cell (E) and carry less information per spike (F), as compared to CTR place cells (all: t-test, $P < 0.01$). The only measure not showing a significant genotype effect was the maximum firing rate (D). These results are in agreement with previous CA1 recordings in these NR1-KO mice (McHugh et al 1996).

(H) P_{idx} (left; see Experimental Procedures) and S_{idx} (right) per animal across sessions (in blocks) for CTR (blue tone symbols) and NR1-KO (red tone symbols).

(I) P_{idx} and S_{idx} , where the departure arm in the latter one was excluded, such that the area covered in both indexes is similar, thus allowing a direct comparison between them. There was a significant genotype and trial type effect (ANOVA: $P(geno) < 0.01$, $P(trial\ type) < 0.01$; horizontal bars indicate significant Post-Hoc differences ($P < 0.05$)).

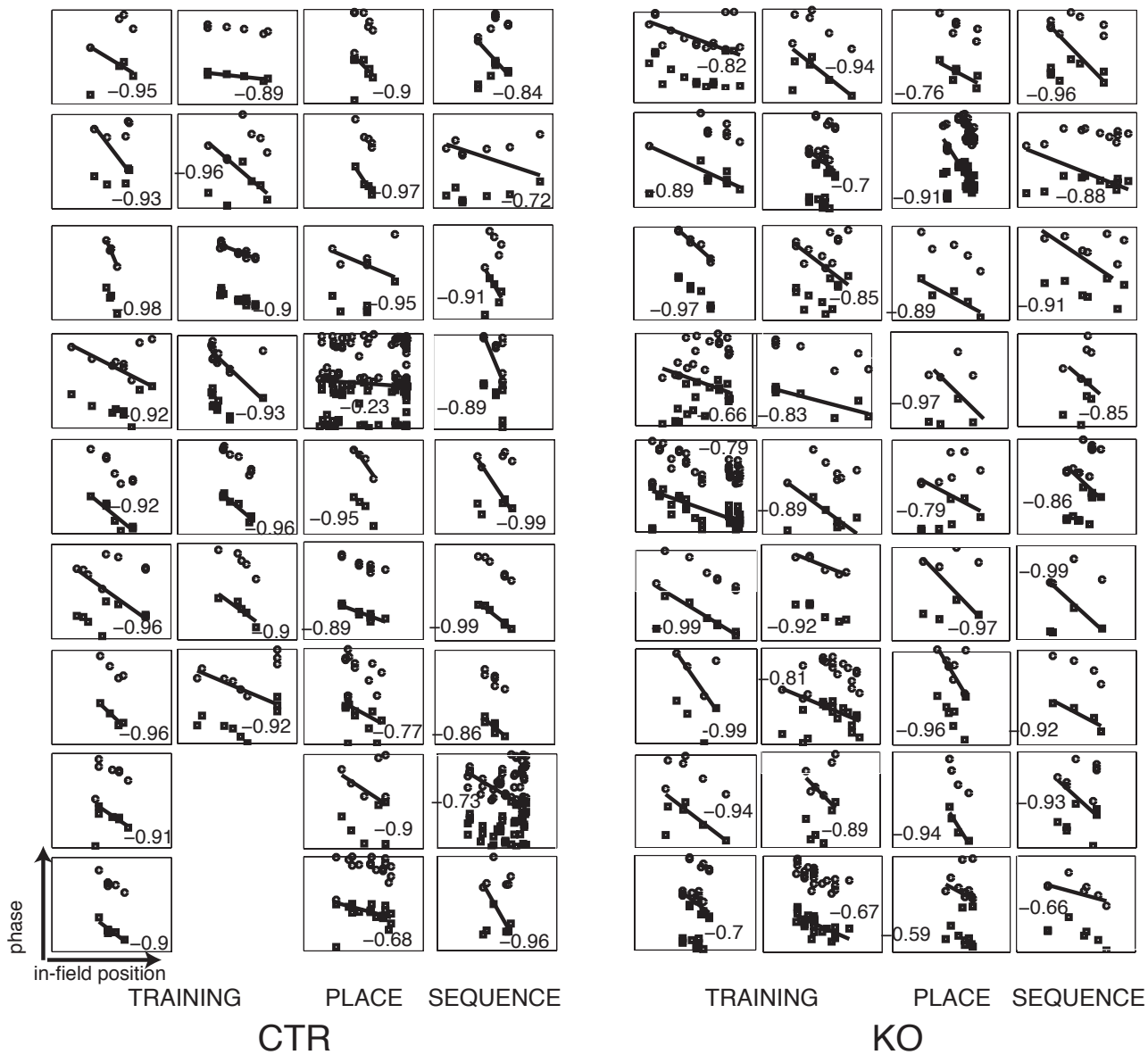

Figure S4. Further examples of single-trial phase precession events in CTR (left) and NR1-KO (right) mice, Related to Figure 6.

Each plot displays the phase as a function of relative mouse position in the cell's place field. Phases are displayed over 2 cycles, for clarity (θ,$\theta + 2 * \pi$). The line corresponds to a circular-linear fit of position *vs* phase (see Experimental Procedures). Value in the plot corresponds to the Pearson's correlation. Columns are divided according to trial type.

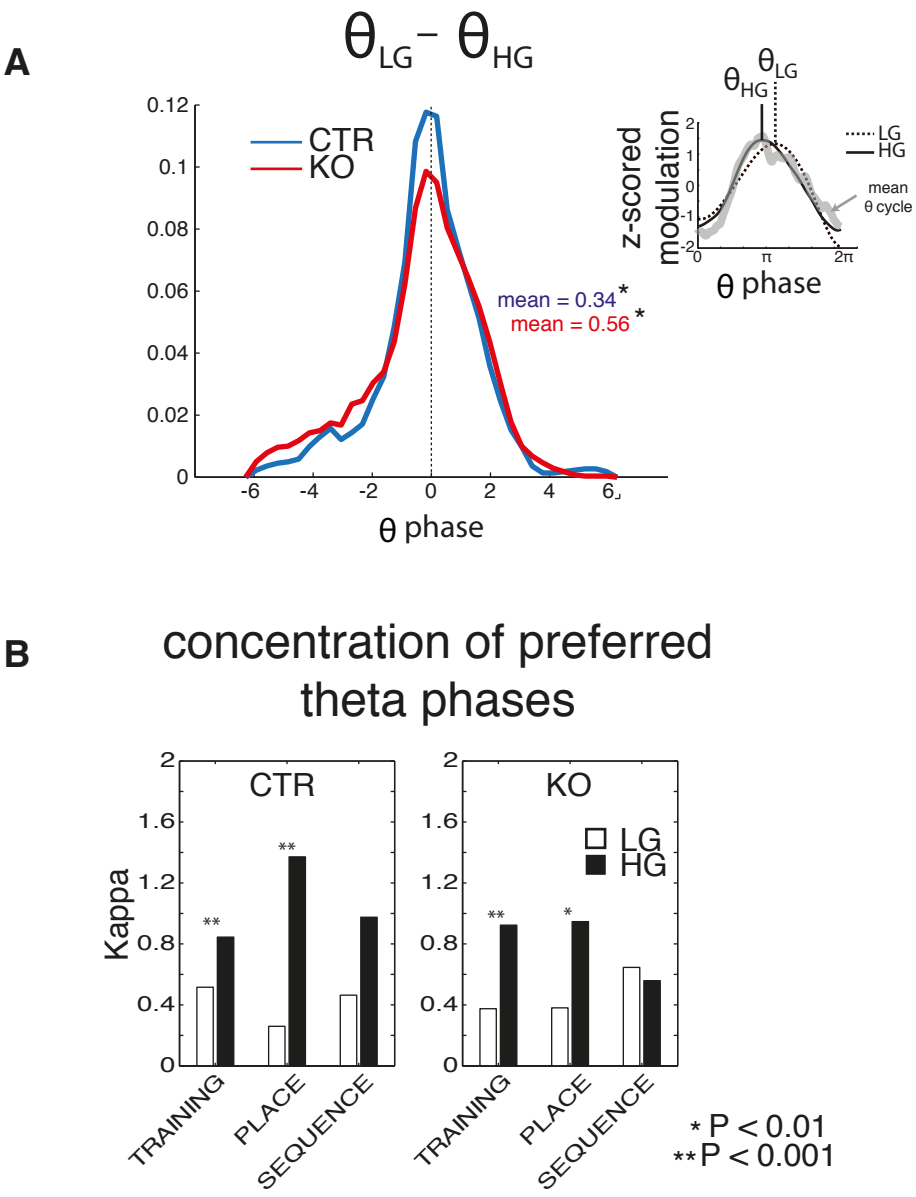

Figure S5. Theta modulation of low and high gamma, Related to Figure 7.

A) Peak modulation of HG preceded that of LG. The preferred phase of LG and HG theta modulation was taken for each trial (a, inset) and the difference between them calculated. In both genotypes the distribution was skewed to positive values (Circular M-test: $P < 0.05$)

B) Concentration of modulation phases as Von Mises kappa. Preferred modulation phases were more concentrated for HG, compared to LG. This was the case for all trial types in CTR (non significant in sequence-strategy trials, but trending). NR1-KO showed a similar pattern, except in sequence-strategy trials, where the concentration of phases was similar for LG and HG.

SUPPLEMENTAL EXPERIMENTAL PROCEDURES

Subjects. Male mice lacking the NMDAR1 gene in the CA1 subregion of the hippocampus, originally created at MIT (Cambridge, Massachusetts) (Tsien et al., 1996a), were inbred in and obtained from Université Paris VI. The KO is specific to the CA1 subfield until 2.5 months of age (Fukaya et al., 2003). Control (CTR) mice were 'floxed' litter-mates of KOs, not carrying the NR-1 deletion. Animals were maintained on a reversed day/night cycle, single-housed and food restricted to 90% of their *ad-libitum* feeding weight. All experiments were carried out in accordance with Dutch National Animal Experiments regulations (*Wet op Dierproeven*) and approved by the Universiteit van Amsterdam. Fifteen mice (8 NR1-KOs and 7 CTRs), were used for electrophysiological experiments, and implanted at the age of 41 ± 5 days, weighing approximately 20 grs. All mice were between 42 (minimum) and 63 (maximum) days of age during the recording phase. At all times, a KO and a CTR mouse were studied in parallel, with all procedures counterbalanced by genotype.

Apparatus. Training took place in a custom made starmaze (Rondi-Reig et al., 2006) (segment dimensions 7 x 20 x 35 cm – for central alleys or 37 cm – for radial arms), with lexan transparent walls. The experimental room had black curtains at the walls with large geometrical cues on the four sides, and 40 watts light bulbs at each corner. Two exemplars of each wall cue were presented to ensure that radial arm identification could not be accomplished by seeing any single visual cue.

Behavioral Protocol. In training trials, animals had to navigate to the goal arm leaving from a fixed departure arm (Figure 1A). Probe trials were administered to assess the behavioral strategy used by the animals. In these trials, the animal was set to depart from a different arm, no effort being made to disorient the animals. Depending on the trajectory used by the mouse, each trial was attributed to a different strategy: a probe trial resulting in a run directly to the arm rewarded in training trials was classified as a place-strategy trial, consistent with the animal identifying the goal arm with reference to a map of the environment. If the animal used the same sequence of turns as in training trials (e.g. left-right-left turn), therefore ending in a different arm, this was interpreted as the animal executing a sequence of egocentric movements to reach the goal (sequence) (Figure 1C). During probe trials, both place and sequence choices were rewarded.

Four days after arrival at the lab (average age at arrival: 29.8 ±1.7 days), mice were introduced to a 2-days habituation protocol to the maze.After habituation, pre-training started, consisting of two daily sessions for 5 days (one in the morning, one in the afternoon), each session containing seven training trials, except for the first two sessions, which comprised only 6 trials. From day 3 until the end, trial 5 was a probe trial (FigureS1).

After pre-training, mice underwent drive implant surgery (at all times a CTR/NR1-KO pair was studied in parallel). Eight days after implantation, recordings in the starmaze started with two daily sessions during the first 7 days and a single session on the 8th day (total:15 sessions). Each session contained 15 training trials; probe trials were introduced in session 2 (one probe trial in session 2 and 3 probe trials thereafter). Each session was flanked by two rest or sleep periods (at least 20 min long). For electrophysiological recordings, a new configuration of departure and goal arms was chosen, and a new set of environmental cues was used.

A visit to an unrewarded arm was considered a mistake. After two mistakes, the trial was terminated and the mouse was returned to its home cage. During a ~1 minute inter-trial interval, the experimenter wiped the maze with a 20% ethanol solution. Each recording session was flanked by 20 minutes sleep periods that were used to assess recording stability.

*Drive, Surgery and Tetrode positioning.*Six independently moveable tetrodes were loaded into a custom made Microdrive (Battaglia et al., 2008), implanted over the dorsal hippocampus (AP: -2.0 mm, ML: -2.0 mm). In the week after surgery, tetrodes were gradually lowered until they reached the CA1 pyramidal layer, before recordings began. Tetrode position was adjusted between recording sessions to maintain them in the CA1 pyramidal layer, which was identified by the presence of strong ripple events and the presence of bursty excitatory neurons.

Histology. After recordings, electrolytic lesions were made at the recording sites by passing 20 μA of current for 10 s through one lead of each tetrode. After perfusion with formal saline, coronal brain sections (40μm) were cut on a Vibratome and Nissl-stained for verification of tetrode tracks and end points. Only animals with clear lesions in the CA1 pyramidal layer and/or clear sharpwave-ripple complexes and ripple-modulated cells firing were included in the analysis.

Data acquisition. Tetrode signals were unit-gain amplified by the headstage pre-amplifiers (Neuralynx, Bozeman, MT) and relayed to amplifiers for single-unit and local field potential (LFP) recordings. The signal was amplified 2000 times, bandpass filtered (0.6–6.0 kHz for single-unit; 1-475 Hz for LFP), acquired (sampling rate: 32 kHz for threshold-triggered spike waveform acquisition; continuously at 2 kHz for LFP) and time-stamped. A tetrode (targeted to a location devoid of units and near the area of interest, like the corpus callosum) was used as a reference.

Single-unit data were pre-processed with KlustaKwik (Harris et al., 2000) for automated spike clustering. Spike sorting results were manually refined, using Klusters (Hazan et al., 2006).

Mouse position and orientation on the maze were extracted from video footage (using the full animal silhouette as filmed by a camera placed directly on top of the maze) with Ethovision XT image analysis software (Noldus, Wageningen, The Netherlands), which was synchronized with the electrophysiology data acquisition system.

Data analysis: Behavior. To quantify performance in the starmaze, we used the localization score (Fouquet et al., 2011), calculated by evaluating the animal's choice at each intersection: a choice bringing it closer to the goal was awarded a value of 100 (0 otherwise). Values from every intersection were averaged to obtain a per-trial value, and the result of all training trials in a session was averaged, to obtain a score for that session. Because there are two possible paths to goal (short and long, see Figure1A), the choice at the first intersection was always awarded 100. For the strategy identification in probe trials, only probe trials that were preceded by at least 2 equivalent correct training trials (e.g., for a short sequence probe trial, a minimum of 2 short training trials) since the previous probe trial, were considered.

Data analysis: electrophysiology. All data used for analysis were from periods in which the animal was moving at speeds exceeding 3 cm/sec.

To address the similarity of the firing rate maps between training and probe trials, we calculated two different indices. For place-strategy trials, we extracted the common occupancy area between a training and a place-strategy trial. For cells with at least two thirds of its training trial place field in the common area, we calculated the P_{idx}, i.e. the Pearson's correlation between its firing map in the two conditions in that area.

The $S_{idx}$was computed similarly, but first the mouse's occupancy map in sequence-strategy trials was rotated by the angle difference between the departure arms in training trials and in probe trials (360^o / 5 = 72^o) and aligned to match the occupancy map of the training trials. Sequence-strategy trials making use of 'short' and 'long' trajectories were compared with their training trial equivalents (Figure 3A,B).

To normalize the correlation, accounting for the small differences in place field size across genotypes, we formed a shuffled data set by calculating the correlation between the firing map in training trials for a given cell with the firing map in probe trials for a different cell. This procedure was repeated for all possible cell pairs of mice of the same genotype and the average value was used for the normalization.

Spectral power analysis. A notch filter was applied to the LFP trace, around 50 Hz (49-51 Hz) and its 2^{nd} and 3^{rd} harmonic. Power spectra were constructed on a trial-by-trial basis, to allow comparison with probe trials, using the Chronux toolbox (http://www.chronux.org), between 0 and 150Hz, using 5 tapers (NW=3) and in windows of 1sec.

For the construction of the normalized power plots in Figure 4B, the power spectrum of each trial was divided by the mean power between 4 and 140 Hz.

For the construction of the log ratio power plots in Figure 4C and D, the power spectrum of place and sequence-strategy trials were divided by the average of the power spectra of the correct trials in that session. The 5^{th} and 95^{th} percentiles of the shuffled data were obtained by bootstrapping 2000 times the ratio between a trial

taken randomly among the correct, place and sequence-strategy trials of each session and dividing it by the average power of the correct trials of that session.

The low to high gamma ratios in figure 4E were obtained from the raw power spectrum.

Spike-LFP PPC analysis. The circular concentration of spike-LFP phases was quantified using the pairwise phase consistency (PPC) (Vinck et al., 2010). For a given frequency *f*, we determined the instantaneous spike-LFP phases by Fast Fourier Transforming a Hann-tapered LFP segment around the spike, with length $5/f$ seconds, thereby maintaining a constant frequency resolution at any frequency *f.* We denote the spike-LFP phase for the i-th spike in the m-th trial at frequency *f* by $\theta_{i,m}$. For single trial analysis, we computed the PPC as in ref. (Vinck et al., 2011a) by

$$ppc_0 = \frac{\sum_{j=1}^{N_m}\sum_{k\neq j}^{N_m}\left(\sin(\theta_{j,m})\sin(\theta_{k,m}) + \cos(\theta_{j,m})\cos(\theta_{k,m})\right)}{N_m(N_m-1)} \quad (1),$$

where N_m denotes the number of spikes in trial *m*. If multiple trials were available, we computed the PPC (Vinck et al., 2011a) by

$$ppc_1 = \frac{\sum_{m=1}^{M}\sum_{l\neq m}^{M}\sum_{j=1}^{N_m}\sum_{k=1}^{N_m}\left(\sin(\theta_{j,m})\sin(\theta_{k,l}) + \cos(\theta_{j,m})\cos(\theta_{k,l})\right)}{\sum_{m=1}^{M}\sum_{l\neq m}^{M} N_m N_l} \quad (2).$$

The PPC considers one pair of spike-LFP phases at a time and determines to what degree this pair of spike-LFP phases is coincident or not, using the dot product. Because PPC is a pairwise measure, it is not biased by the number of spikes. Furthermore, is not affected by non-Poissonian history effects within spike trains, such as bursting, autorhythmicity or a refractory period (Vinck et al., 2012). The expected value of the PPC equals the squared phase-locking value (i.e., the resultant length of the spike phases; Vinck et al., 2012). We only considered spike-LFP pairs recorded on two different tetrodes. Significance of phase locking (18-100 Hz) was assessed using cluster-mass based permutation statistics (Bullmore et al., 1999; Maris et al., 2007): each individual frequency was tested for significant locking using the Rayleigh test(at $P < 0.05$)then the cluster-mass of aligned, significant PPC (eq. 2) values was taken as the test statistic, thereby correcting for multiple comparisons across frequencies.

Single trial phase precession analysis. Phase precession was calculated on a trial-by-trial basis (Schmidt et al., 2009). Mouse paths were linearized and the firing rate calculated as a function of distance from departure. Single-trial place fields were determined by detecting adjacent bins (bin=4cm) where cell activity was above 1/3 of the trial's maximum firing rate and with

at least 4 spikes. The theta phase for each spike was determined using the Hilbert's transform of the filtered (7-10Hz) LFP signal. Taking θ_i and x_i as respectively the theta phase and the position on the track for the *i*-th spike, an estimate of the slope, $\hat{a}$, was calculated by maximizing the resultant length

$$R(a) = \sqrt{\left(\frac{1}{n}\sum_{j=1}^{n}\cos(\theta_j) - 2\pi a x_j\right)^2 + \left(\frac{1}{n}\sum_{j=1}^{n}\sin(\theta_j) - 2\pi a x_j\right)^2} \quad (3)$$

where *n* is the number of spikes, over the range [-4π:0]. Restricting the values of *a* to this range avoids fitting lines with arbitrarily high values or with positive slopes.

The phase range of the precession R_φ is then calculated from the slope and the 'place field size' R_p, defined as the distance between the 1st and the last spike:

$$R_\varphi = \hat{a} * R_p \quad (5)$$

For the correlation strength of the phase precession fit, a multiple of 2π was added to each θ_i in order to minimize the residues of the linear-circular fit and the (linear) Pearson's correlation coefficient between θ_i and x_i was then taken (Figure 6B).

Circular statistical analyses(Figure6 and 7) were performed using the Circular Statistics Toolbox for Matlab (Berens et al, 2009).

Spatial representation during periods of low and high gamma. The EEG signal was filtered in the theta band (6-12Hz) and the troughs of the filtered traced were detected. For each theta cycle, the log-ratio between the power in the LG (23-40Hz) and the HG(55-90Hz) bands was taken. Theta cycles falling in the first and last quartiles were taken as periods of predominant HG and LG, respectively. These intervals were used to construct firing maps for each cell during place and sequence probe trials. The resulting maps were normalized by a shuffling condition, similar to the analysis in Figure 3 A and B, and were then correlated with the firing maps during all periods of the corresponding training trials (like the P_{idx} and S_{idx}).

SUPPLEMENTAL BIBLIOGRAPHY

Philipp Berens. Circstat: A matlab toolbox for circular statistics. Journal of Statistical Software, 31(10):1–21, 9 2009. URL http://www.jstatsoft.org/v31/i10.

Bullmore, E.T., Suckling, J., Overmeyer, S., Rabe-Hesketh, S., Taylor, E., and Brammer, M.J. (1999). Global, voxel, and cluster tests, by theory and permutation, for a difference between two groups of structural MR images of the brain. IEEE Trans Med Imaging *18*, 32-42.

Fukaya, M., Kato, A., Lovett, C., Tonegawa, S., and Watanabe, M. (2003). Retention of NMDA receptor NR2 subunits in the lumen of endoplasmic reticulum in targeted NR1 knockout mice. Proc Natl Acad Sci U S A *100*, 4855-4860.